Langmuir

ARTICLE

pubs.acs.org/Langmuir

Correlation between the Structure and Wettability of Photoswitchable Hydrophilic Azobenzene Monolayers on Silicon

Xiaowei Pei,[†] Antony Fernandes, Bertrand Mathy, Xavier Laloyaux, Bernard Nysten, Olivier Riant, and Alain M. Jonas*

Institute of Condensed Matter and Nanosciences, Université Catholique de Louvain, Croix du Sud 1/4, 1348 Louvain-la-Neuve, Belgium

ABSTRACT: Photoresponsive monolayers of hydrophilically substituted azobenzenes have been prepared by reaction on aminosilane monolayers on silicon surfaces. Grafting densities in the 0.2−1.0 molecule/nm^2 range were determined by X-ray reflectometry. The monolayers exhibit reversible photoisomerization, switching from a more hydrophilic trans state to a less hydrophilic cis state upon UV irradiation, in contrast with the usual behavior of most azobenzene monolayers that switch from a less to a more hydrophilic state. This indicates that the wettability is not dominated by the change in the dipole moment of the azobenzene moiety but originates from variations in the composition of the outer surface of the monolayers resulting from the reorientation of the substituent groups. The light-driven change in the water contact angle correlates linearly with the grafting density but remains small. However, the wettability contrast can be increased by forcing the molecules to stand in an improved vertical orientation, either by densifying the underlying aminosilane monolayer or by filling the voids left at the bottom of the layer of grafted azobenzene molecules.

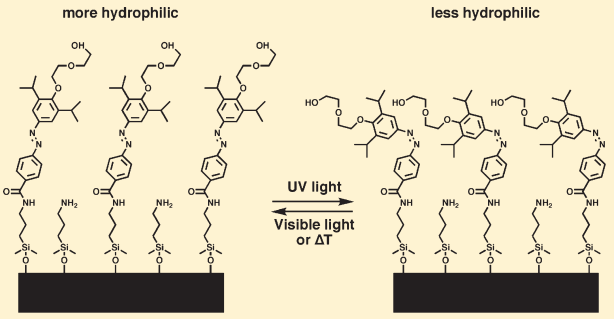

INTRODUCTION

Photoswitchable surfaces are surfaces capable of reversibly changing their properties when illuminated by light of a proper wavelength. The local actuation permitted by light, coupled to its largely innocuous and noninvasive nature, is a strong incentive for the development of such photoswitchable surfaces,[1−3] which find applications in microfluidics,[4] cell culturing,[5,6] catalysis,[7] and photoelectronics.[8] In this context, we have been interested in surfaces displaying reversible changes in wettability upon irradiation because such surfaces can be used to convert light energy directly into mechanical work.[4]

The incorporation of photochromic molecular switches in self-assembled monolayers (SAMs) is a typical methodology for obtaining photoswitchable surfaces. Among the various types of photochromic molecules, azobenzenes are most frequently used[9,10] because of their wide availability and sturdiness. Azobenzene undergoes a trans (E) to cis (Z) isomerization upon UV irradiation ($\lambda \approx 365$ nm), which results in large changes in both the geometry and electric dipole moment. The cis isomer is metastable and returns to the trans configuration spontaneously or upon irradiation with visible light ($\lambda \approx 430$ nm). Two methods are essentially used to prepare azobenzene-containing monolayers. One is the direct chemisorption of azobenzene-bearing reactive molecules on a substrate,[11−18] and the other consists of forming a dense functional monolayer onto which, in a second step, azobenzene units are grafted.[13,19−25]

When grafted in monolayers, azobenzene still exhibits trans to cis isomerization, provided enough free volume is available for the change in configuration to happen: it was found that azobenzene layers are photochemically inactive above a grafting density of ∼2.5 molecule/nm^2.[3] Therefore, dense self-assembled monolayers such as those obtained by the deposition of thiols on crystalline gold need to be tailored to decrease the packing density of azobenzenes (e.g., by mixing azobenzene-bearing thiols with shorter alkane thiols[26,27] or by using unsymmetrical azobenzene disulfides[16,18,28−30]). Another strategy is to prepare azobenzene-based SAMs from solution under UV-light irradiation; under this condition, the solution is enriched in cis isomers leading to SAMs with increased free volume.[31] In contrast, monolayers of azobenzene silanes on silicon oxide are usually less dense because of the amorphous nature of silicon oxide and the lateral requirements of siloxane bonds. These monolayers are intrinsically more disordered, and the azobenzene units thus have a less-well-defined orientation. Despite these limitations, silicon oxide surfaces remain attractive because thiol monolayers have limited thermal stability[32] and are prone to exchange reactions.[33]

The variation of the wettability of azobenzene SAMs upon UV irradiation is frequently ascribed to the large difference between the molecular dipole moments of the cis and trans configurations (generally on the order of 2 to 3 D depending on substitution)[16,19] or to the more vertical orientation of the net dipole moment at cis-enriched surfaces.[34] This view is globally supported by the observation that water generally has a lower contact angle on cis-enriched than on trans-rich monolayers.[35]

Received: April 25, 2011
Revised: June 17, 2011
Published: June 23, 2011

Scheme 1. Schematic Illustration of the Reversible Photoisomerization Process of a Hydrophilic Azobenzene Monolayer (Grafted onto an Aminosilane Monolayer), Switching the Surface from a More to a Less Hydrophilic State upon UV Irradiation

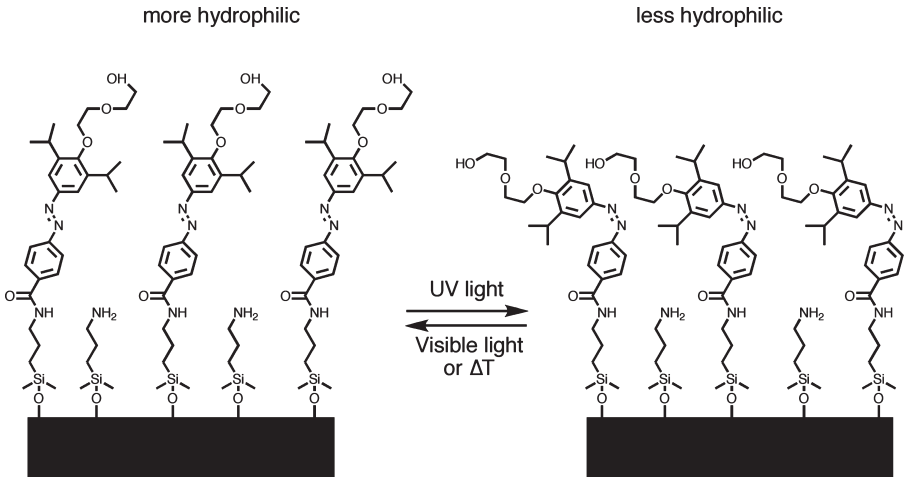

The measured surface tensions of 4′-pentyl-azobenzene monolayers in trans and cis configurations, which are 35 and 40 mJ/m^2, respectively, also provide support for this interpretation.[19] However, the variations in the water contact angles are invariably modest, below ∼10°,[3] except when the surfaces are properly roughened in order to benefit from superhydrophobicity or superhydrophilicity.[36] Here, however, we do not want to use rough surfaces because these would not be compatible with the nanolithography processes that we plan to use at a later stage in our research. In addition, we are interested in surfaces having the stable (trans) state more hydrophilic than the metastable (cis) state, in contrast to previous observations.[35] In other words, we want to have an increase in the water contact angle upon UV irradiation, whereas the opposite behavior is generally reported.

This should be possible provided the change in wettability under UV irradiation is not dominated by the change in the dipole moment of the switching azobenzene unit but instead results from the change in orientation of functional units grafted to the azobenzene and from the possible resulting variation in chemical composition of the outmost surface. In such a case, by substituting the para position of the top azobenzene unit with hydrophilic moieties and its meta positions with hydrophobic ones, it should be possible to have a more hydrophilic monolayer in the trans state, switching to a less hydrophilic one in the cis state (Scheme 1). Obviously, the possibility to expose the desired groups will depend strongly on our ability to fix the molecules in upright positions while still maintaining sufficient free volume in the layer to allow isomerization to occur, which is directly related to the method of preparation of the monolayers.

In this article, we will thus explore monolayers of azobenzene molecules substituted with various hydrophilic groups in the para position, prepared under different conditions in order to vary their grafting density and to force them to stand upright as much as possible. Importantly, the novel azo-SAMs described in this work are all relatively hydrophilic, in contrast to those in previous work. We show that monolayers switching from a more to a less hydrophilic state when irradiated with UV light can indeed be prepared, and we correlate the observed variation in contact angle with the grafting density of the azobenzene units measured by X-ray reflectometry. From these observations, we finally design improved photoswitchable monolayers with an enhanced wettability contrast between the cis and trans forms.

EXPERIMENTAL SECTION

Materials. All chemicals and solvents were purchased from Sigma-Aldrich, Acros Organics, or ABCR and used without further purification. Column chromatography was performed on ROCC 60 granular silica gel (40−63 μm, 230−400 mesh ASTM). Single-side-polished silicon wafers were obtained from ACM (France) with a (100) orientation; they were cut into squares with 1.5 cm sides. Milli-Q water (resistivity 18.2 MΩ cm) was obtained from a Millipore system.

Synthesis. The synthesis route for azobenzene derivatives used in this study is illustrated in Scheme 2 and was carried out as follows.

*Ethyl 4-(2′,6′-Diisopropyl-4′-hydroxyphenylazo) Benzoate (**1**).* Ethyl 4-aminobenzoate (4.95 g, 30.0 mmol) was added to a solution of concentrated HCl (9 mL) in water (9 mL) at 0 °C and stirred vigorously for 30 min. Sodium nitrite (2.07 g, 30.0 mmol) in distilled water (60 mL) was added dropwise to the reaction mixture, and the solution was stirred for 1 h at 0 °C. KOH (2.52 g, 45.0 mmol) and 2,6-diisopropylphenol (5.35 g, 30.0 mmol) were dissolved in methanol (60 mL) and stirred for 30 min at 0 °C. The former solution was added dropwise to the latter, and the reaction was stirred for 5 h at 0 °C. After extraction with dichloromethane, the organic layer was washed with distilled water and then evaporated under reduced pressure. The crude product was recrystallized twice from ethanol at 0 °C, yielding a red-brown powder (8.10 g, yield 76%). ^{1}H NMR (300 MHz, DMSO-d_6) δ 9.19 (bs, 1H, O*H*), 8.11 (d, 2H, J = 8.4 Hz, Ar−*H*), 7.92−7.89 (m, 2H, Ar−*H*), 7.66 (s, 2H, Ar−*H*), 4.34 (q, 2H, J = 7.2 Hz, COOC*H*$_2$CH$_3$), 3.38−3.33 (m, 2H, C*H*(CH$_3$)$_2$), 1.34 (t, 3H, J = 7.2 Hz, COOCH$_2$C*H*$_3$), 1.22 (d, 6H, J = 6.9 Hz, CH(C*H*$_3$)$_2$), 1.13 (d, 6H, J = 6.9 Hz, CH(C*H*$_3$)$_2$). ^{13}C NMR (75 MHz, DMSO-d_6) δ 165.2, 155.5, 145.7, 135.9, 130.4, 122.2, 119.0, 60.9, 26.3, 22.7, 14.2. MS (APCI) m/z 355.1 [M + H]$^+$.

*4-(2′,6′-Diisopropyl-4′-((ω-hydroxyethoxy)ethoxy)phenylazo) Benzoic Acid (**2**).* A mixture of **1** (1.78 g, 5.0 mmol), 2-(2-chloroethoxy) ethanol (1.00 g, 8.0 mmol), K_2CO_3 (3.00 g), and KI (50 mg) in dry acetone (50 mL) was heated under reflux for 3 days under N_2. The reaction was cooled to room temperature and filtered. The filtrate was concentrated under reduced pressure, and the residue was purified by column chromatography (SiO_2) with hexane/EtOAc (3:1 v/v) as the eluent to give an orange solid. The solid was further dissolved in a solution of KOH (2.00 g) in ethanol (60 mL) and heated under reflux overnight. The mixture was then cooled to room temperature and

dx.doi.org/10.1021/la201526u |*Langmuir* 2011, 27, 9403–9412

Scheme 2. Synthesis of the Azobenzene Derivatives Used in This Work

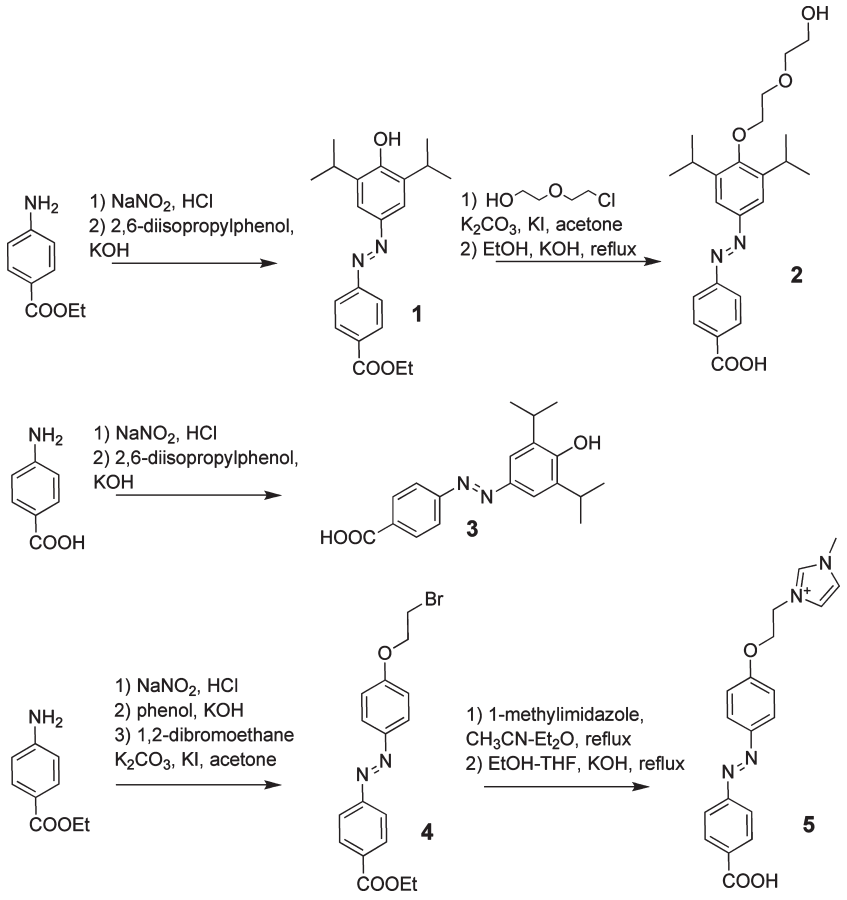

poured into 1 M HCl at 0 °C. After filtration, the crude product was washed with water and dried under vacuum. The sample was recrystallized twice from ethanol to give a yellow powder (1.17 g, yield 56%). ^{1}H NMR (300 MHz, DMSO-d_6) δ 13.19 (bs, 1H, COO*H*), 8.13 (d, 2H, J = 8.4 Hz, Ar−*H*), 7.95 (d, 2H, J = 8.4 Hz, Ar−*H*), 7.72 (s, 2H, Ar−*H*), 4.63 (bs, 1H, O*H*), 3.93 (s, 2H, OC*H*$_2$CH$_2$OCH$_2$CH$_2$OH), 3.79 (s, 2H, OCH$_2$CH$_2$OCH$_2$C*H*$_2$OH), 3.55 (s, 4H, OCH$_2$C*H*$_2$OC*H*$_2$CH$_2$OH), 3.44−3.38 (m, 2H, C*H*(CH$_3$)$_2$), 1.24 (d, 12H, J = 6.9 Hz, CH(C*H*$_3$)$_2$). ^{13}C NMR (75 MHz, DMSO-d_6) δ 166.7, 156.4, 148.9, 143.1, 130.6, 122.4, 119.0, 74.1, 72.4, 69.6, 60.3, 26.0, 23.7. MS (APCI) m/z 415.1 [M + H]$^+$.

*4-(2′,6′-Diisopropyl-4′-hydroxyphenylazo) Benzoic Acid (**3**).* The synthesis of compound **3** is similar to that of **1** and gives an orange crystalline powder. ^{1}H NMR (300 MHz, DMSO-d_6) δ 13.11 (bs, 1H, COO*H*), 9.16 (bs, 1H, O*H*), 8.10 (d, 2H, J = 8.1 Hz, Ar−*H*), 7.90 (d, 2H, J = 8.4 Hz, Ar−*H*), 7.67 (s, 2H, Ar−*H*), 3.39−3.35 (m, 2H, C*H*(CH$_3$)$_2$), 1.23 (d, 12H, J = 6.6 Hz, CH(C*H*$_3$)$_2$). ^{13}C NMR (75 MHz, DMSO-d_6) δ 166.8, 155.4, 154.7, 145.7, 135.9, 131.7, 130.5, 122.1, 118.9, 26.3, 22.7. MS (APCI) m/z 327.1 [M + H]$^+$.

*Ethyl 4-(4′-Bromoethyloxyphenylazo) Benzoate (**4**).* Ethyl 4-(4′-hydroxyphenylazo) benzoate was first synthesized according to the route described for compound **1** and recrystallized twice from ethanol. A mixture of ethyl 4-(4′-hydroxyphenylazo) benzoate (1.35 g, 5.0 mmol), 1,2-dibromoethane (1.50 g, 8.0 mmol), K_2CO_3 (3.00 g), and KI (50 mg) in dry acetone (50 mL) was heated under reflux for 3 days under N_2. The resulting mixture was cooled to room temperature and filtered, and the filtrate was concentrated under reduced pressure. The product was precipitated with ethanol, filtered, and purified by column chromatography (SiO_2) with hexane/dichloromethane (1:1 v/v) as the eluent to give ethyl 4-(4′-bromoethyloxyphenylazo) benzoate as a yellow solid. ^{1}H NMR (300 MHz, $CDCl_3$) δ 8.18 (d, 2H, J = 8.7 Hz, Ar−*H*), 7.96 (d, 2H, J = 9.0 Hz, Ar−*H*), 7.91 (d, 2H, J = 8.7 Hz, Ar−*H*), 7.04 (d, 2H, J = 9.0 Hz, Ar−*H*), 4.45−4.38 (m, 4H, COOC*H*$_2$CH$_3$, OC*H*$_2$CH$_2$Br), 3.69 (t, 2H, J = 6.3 Hz, OCH$_2$C*H*$_2$Br), 1.43 (t, 3H, J = 7.2 Hz, COOCH$_2$C*H*$_3$). ^{13}C NMR (75 MHz, $CDCl_3$) δ 163.7, 159.6, 153.2, 145.2, 129.9, 128.8, 123.5, 120.7, 113.5, 66.6, 59.3, 28.5, 12.7. MS (APCI) m/z 377.0, 379.0 [M + H]$^+$.

*1-((4-(4′-Carboxyphenylazo)phenyloxy))ethyl-3-methyl-imidazolium Bromide (**5**).* Ethyl 4-(4′-bromoethyloxyphenylazo) benzoate **4** (2.07 g, 5.5 mmol) and 1-methylimidazole (0.41 g, 5.0 mmol) were dissolved in dry diethyl ether (10 mL) and acetonitrile (15 mL). The mixture was vigorously stirred and refluxed in the dark for 24 h under N_2. After the mixture was cooled to room temperature, the solvent was evaporated under reduced pressure and the solid residue was carefully washed with diethyl ether. The crude product was recrystallized from ethanol to give a red-brown solid that was further dissolved in a solution of KOH (1.00 g) in ethanol (20 mL) and THF (15 mL) and heated under reflux overnight. The mixture was then cooled to room temperature and poured into 1 M HCl at 0 °C. After filtration, the crude product was recrystallized twice from ethanol to give an orange powder. ^{1}H NMR (300 MHz, CD_3OD) δ 9.11 (s, 1H, imidazolium ring), 8.16 (d, 2H, J = 8.7 Hz, Ar−*H*), 7.94 (d, 2H, J = 9.0 Hz, Ar−*H*), 7.90 (d, 2H, J = 8.7 Hz, Ar−*H*), 7.77 (s, 1H, imidazolium ring), 7.62 (s, 1H, imidazolium ring), 7.14 (d, 2H, J = 9.0 Hz, Ar−*H*), 4.71 (t, 2H, J = 4.5 Hz, NC*H*$_2$), 4.51 (t, 2H, J = 4.5 Hz, OC*H*$_2$), 3.97 (s, 3H, N−C*H*$_3$). ^{13}C NMR (75 MHz, CD_3OD) δ 162.3, 156.6, 148.8, 138.6, 131.8, 126.2, 125.0, 124.3, 123.4, 116.1, 67.5, 50.2, 36.6.

Preparation of the Monolayers. *Cleaning of the Silicon Wafers.* The silicon substrates covered with an ∼1.5-nm-thick native oxide layer

dx.doi.org/10.1021/la201526u |*Langmuir* 2011, 27, 9403–9412

were cleaned by immersion in a hot, freshly prepared piranha solution (H_2SO_4 (98%)/H_2O_2 (27%) 1:1 v/v) for 40 min. ***Caution!*** *Piranha solution is an extremely strong oxidant and should be handled only with the proper equipment.* The substrates were then extensively rinsed with Milli-Q water and dried under a flow of ultrapure Ar (grade 5.5 from Air Products). The silicon wafers were immediately used in order to prevent surface contamination.

Deposition of the Silane Monolayers. All samples were obtained by grafting activated esters onto monolayers of γ-aminopropyldimethylethoxysilane (APDMS). The APDMS layer was formed by gas-phase silanation in a Schlenk tube at 80 °C as described previously.[37] After reaction, the samples were washed with dichloromethane for 24 h in a Soxhlet apparatus. For one sample, a 1:1 solution of APDMS and *tert*-butyldiphenylchlorosilane (TBDPSCl) in dry toluene (0.25% v/v) was prepared, and the silanation was performed in solution in a glovebox (moisture level below 1 ppm).

N-Hydroxysuccinimide Activation of Azobenzene Carboxylic Acids. *N*-Hydroxysuccinimide-activated azobenzenes were prepared by reacting azobenzene carboxylic acid derivatives **2**, **3**, or **5** with *N*-hydroxysuccinimide (1.1 equiv) in dry DMF in the presence of DCC (1.0 equiv) and DMAP (catalytic amount) for 24 h. The reaction mixture was filtered, and the filtrate was poured into water to precipitate the NHS-activated esters that were further recrystallized in EtOH and directly used.

Coupling of N-Hydroxysuccinimide-Activated Azobenzene Esters to Aminosilane Monolayers. The silanized substrate bearing terminal amino groups was immersed in a 4 mM THF solution of NHS-activated azobenzene esters at room temperature for 24 h with gentle shaking. The substrate was then removed from the solution and washed thoroughly with THF and EtOH to remove unbound reagent. After being dried with ultrapure Ar, the substrates were stored in vacuum. In one instance, the azobenzene compound was grafted under UV irradiation (360 nm). In this case, the grafting reaction was limited to 2 h and the azobenzene solution was first irradiated for 30 min before being introduced. The substrates were then washed and stored as described above.

*N-Hydroxybenzotriazole-Mediated Coupling of Azobenzene **2** to Aminosilane Monolayers.* The aminosilanized substrate was immersed in a 4 mM THF solution of **2** in the presence of HOBt (10 mM), DCC (10 mM), and DMAP (catalytic amount) at room temperature with gentle shaking for 24 h. Cleaning and drying are as described above.

Sample Characterization. *X-ray Reflectometry (XRR).* XRR measurements were carried out with a modified Siemens D5000 2-circle goniometer (0.002° positioning accuracy). X-rays of 0.15418 nm wavelength (Cu Kα) were obtained from a Rigaku rotating anode operated at 40 kV and 300 mA, fitted with a collimating mirror (Osmic, Japan) delivering a close-to-parallel beam of ∼0.0085° vertical angular divergence. The beam size was defined by a 40-μm-wide slit placed 17.5 cm away from the focal spot. The sample was placed within 2 μm of the center of the goniometer, and the reflected beam was collected through a 200-μm-wide detector slit. Soller slits in the incident and reflected beam limited the axial divergence to 0.02°. The data were corrected for spillover and normalized to unit incident intensity; they are reported as a function of k_{z0}, the vertical component of the photon wavevector in a vacuum.

The XRR data were analyzed in three different ways. First, an estimation of the average thickness of the monolayer, d_x, was obtained from the value of $k_{z,\min}$ in the reflectogram, according to $d_x = \pi/(2k_{z,\min})$. Here, $k_{z,\min}$ is the k_{z0} value corresponding to the first minimum in the reflectivity curve, arising from destructive interference. Second, a Patterson function was computed from the data as described elsewhere,[38,39] from which a second estimation of the average thickness d of the layers was obtained by taking the location of the last maximum in the Patterson function. In addition, the maximal thickness of the layer (including the protrusions arising from the roughness), $d_{\max}$, was taken as the value for which the last peak in the Patterson function goes back to the baseline. Third, the film was modeled as a succession of thin virtual homogeneous layers of zero interfacial roughness, stacked over the Si substrate of electron density held at 700 electron/nm^3. The electron densities ρ_i of the virtual layers were fittable parameters, whereas their widths w_i were held constant at a single value corresponding to the information content of the XRR curves, $w_i = \pi/(2k_{z,\max})$, with $k_{z,\max}$ being the maximal experimental value of k_{z0}. For the experiments reported here, w_i = 0.35 nm. The absorbance of the virtual layers was set to 5×10^{-7} nm^{-1}, and the absorbance of the Si substrate was set to 1.5×10^{-5} nm^{-1}. The initial number of virtual layers was set to $d_{\max}/w_i$; if required, which happened rarely, supplementary slabs were added in the course of the fit. From this model of electron density, the film reflectivity was computed using dynamic theory,[40,41] and the χ^2 function was minimized with a Marquardt−Levenberg algorithm. To avoid numerical problems and unphysical solutions due to the large number of parameters in the final model of the electron density, a regularization technique was applied by adding a smoothing constraint to the χ^2 function, as fully described elsewhere.[39]

The grafting densities were obtained from the electron density profiles $\rho(z)$ in the following way. For silane monolayers, the electron density profile of a clean silicon wafer, $\rho_{Si}(z)$, was subtracted from $\rho(z)$ after horizontal displacement to bring the Si interfaces into agreement. Then, the area below the resulting difference profile was computed, giving access to ζ_g, the total number of electrons belonging to grafted molecules, per unit surface. The grafting density was then obtained as $\sigma_g = \zeta_g/Z$, where Z is the number of electrons in the silane molecule, excluding the reactive ethoxy group. Because of experimental errors in the small thickness of the silane layer and the uncertainty in the lateral shift of one profile versus another, errors of about 20% are to be expected for the values of the grafting density obtained from the density profiles of the silane monolayers. A similar procedure was applied to azobenzene-grafted monolayers; in this case, however, the grafting density was obtained as $\sigma_g = (\zeta_g - \zeta_g')/Z$, where ζ_g' is the number of electrons belonging to the underlying silane monolayer and Z is the number of electrons of the grafted moiety. Because the thickness of these monolayers is larger, the estimated error in the grafting density is lower, in the 10% range.

Photoisomerization. Photoisomerization of the films was carried out by exposure to a 200 W mercury−xenon lamp (Hamamatsu Photonics, L8251) using filters of 90 nm bandwidth centered at 360 nm for UV light and 450 nm for visible light. The terminus of the light guide fiber was set 10 cm above the sample surface to spread the light and to allow irradiation of the entire film area at all times. The measured light intensity at the sample was kept at less than 4 mW/cm^2 to minimize the degradation of the sample by the beam. Immediately after irradiation, contact angles were measured by placing five droplets at different sample locations.

X-ray Photoelectron Spectra (XPS). XPS measurements were performed with an SSX 100/206 photoelectron spectrometer from Surface Science Instruments (USA) equipped with a monochromatized microfocused Al X-ray source (powered at 20 mA and 10 kV). The samples were stuck on a ceramic carousel with double-sided conductive tape; an 8 eV electron flood gun was used to avoid charging. The angle between the surface normal and the axis of the analyzer lens was 55°. The analyzed area was approximately 1.4 mm^2, and the pass energy was set at 150 and 50 eV for survey and elemental scans, respectively. The *C*−(C,H) component of the C 1s peak of carbon was fixed to 284.8 eV to set the binding-energy scale.

Static water contact angles were measured at ambient temperature using the sessile drop method and image analysis of the drop profile. The instrument, using a CCD camera and an image analysis processor, was from Electronisch Ontwerpbureau De Boer (The Netherlands). The Milli-Q water droplet volume was 0.3 μL, and the contact angle was

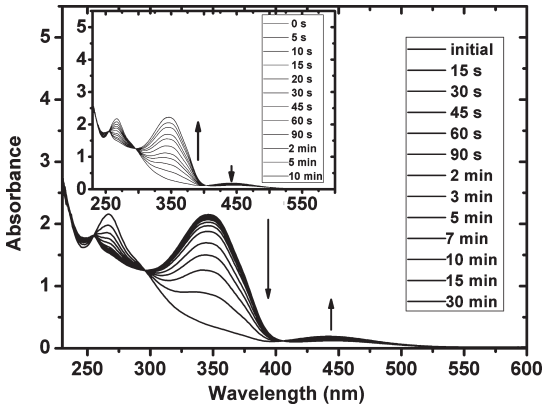

Figure 1. UV−vis absorption spectra of azobenzene **2** in THF (8.0×10^{-5} M) upon irradiation with UV light centered on 360 nm. The inset shows that the cis isomer solution of **2** undergoes cis to trans back-isomerization upon irradiation with visible light centered on 450 nm.

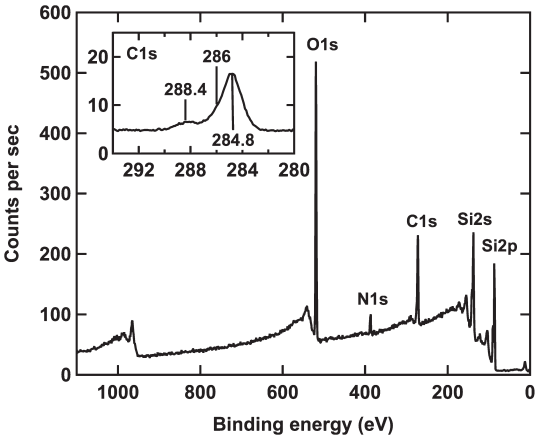

Figure 2. XPS spectrum of NHS-activated azobenzene **2** grafted to an aminosilane monolayer. The inset is a high-resolution XPS spectrum of the C 1s region of the same sample.

measured 5 s after the drop was deposited on the sample. For each sample, the reported value is the average of the results obtained on at least five droplets.

NMR spectra were recorded on a Bruker-300 spectrometer. Chemical shift values for ^{1}H and ^{13}C are referenced to the residual solvent resonances.

Mass spectra were obtained using a ThermoFinnigan LCQ Quantum spectrometer.

UV−vis−NIR absorption spectra of the solution and SAMs were recorded with a Varian Cary 500 scan UV−vis−NIR spectrophotometer. Compound **2** was dissolved in THF at a concentration of 8.0×10^{-5} mol/dm^3 for the measurement in solution.

RESULTS AND DISCUSSION

Synthesis and Photochemical Characterization of Azobenzene Molecules. Because the surface free energies of flat solid substrates are determined by the composition of their outermost surfaces at the atomic level, we designed azobenzene compounds **2**, **3**, and **5** (Scheme 2), which when grafted onto surfaces should present an external hydrophilic group. In addition, the outermost surface should be enriched in hydrophobic groups when the azobenzene switches to its cis configuration following UV irradiation (Scheme 1). In contrast to most compounds reported so far, these azobenzenes include a hydrophilic group in the para position and in the case of **2** and **3** carry two additional hydrophobic isopropyl groups in the meta positions.

The synthesis of the compounds was straightforward. For example, azobenzene derivative 4-(2′,6′-diisopropyl-4′-((ω-hydroxyethoxy)ethoxy)phenylazo) benzoic acid (**2**) was synthesized in three steps (Scheme 2 and Experimental Section). First, ethyl 4-(2′,6′-diisopropyl-4′-hydroxyphenylazo) benzoate **1** was prepared via the classical diazo coupling reaction between ethyl 4-aminobenzoate and 2,6-diisopropylphenol. Then, through the alkylation of **1** with 2-(2-chloroethoxy)ethanol followed by ester hydrolysis, compound **2** was obtained. The photochemical isomerization of **2** was measured with a UV−vis−NIR spectrophotometer. Figure 1 shows the changes in absorption of **2** in THF (8.0×10^{-5} M) upon successive illumination with UV light centered on 360 nm and then with visible light centered on 450 nm. The strong absorbance band at 348 nm is due to the azo $\pi-\pi^*$ electronic transition, and the weaker band at 445 nm is due to the $n-\pi^*$ transition.

Upon irradiation with UV light, the intensity of the $\pi-\pi^*$ transition decreases progressively until a photostationary state is eventually reached. Simultaneously, the intensity of the $n-\pi^*$ transition slightly increases. The existence of isosbestic points at 298 and 407 nm is characteristic of the existence of two distinct absorbing species in equilibrium with each other, confirming the trans−cis isomerization. The conversion in the cis form is close to complete, indicating that the reverse thermal isomerization is slow. The inset picture shows that the cis isomer solution undergoes back-isomerization upon irradiation with visible light. Note that the finally recovered absorption of the trans isomer is slightly higher than that before UV irradiation, which suggests that the initial solution might not fully consist of trans isomers.

Growth and Structural Characterization of Monolayers of Azobenzene Molecules. The grafting of the azobenzene units in monolayers required first activating the carboxylic acid end group of the azobenzene by reaction with *N*-hydroxysuccinimide in the presence of DCC and DMAP. Then, the NHS-azobenzenes were reacted with aminosilanes either in solution or in monolayers. Preliminary experiments indicated that azobenzene silanes led to irreproducible results, certainly as a result of the difficulty in preparing azobenzene silanes of high purity, or to the formation of gels.[14] Therefore, the aminosilane was first grafted onto the substrates, and the azobenzene moieties were subsequently reacted over the monolayers.

To avoid the formation of gels, the monofunctional APDMS aminosilane was used and deposited from the gas phase, giving access to reproducible layers with a grafting density of ~2.7 molecule/nm^2 as determined by XRR (Figure 3, sample s1). This grafting density is about 50% lower than the values found for very densely packed alkane chains; for instance, crystalline alkanes have a packing density of about 5.0−5.5 chains/nm^2 measured in planes perpendicular to the chain axes, depending on their subcell.[42] The relatively low APDMS grafting density results from the dimethyl substitution of the Si atom that prevents the close packing of the chains, from the amorphous nature of the native layer of silicon oxide on silicon wafers, and from the intrinsically more disordered nature of silane monolayers grafted at a relatively high temperature from the gas phase (80 °C). However, this experimental grafting density is close to

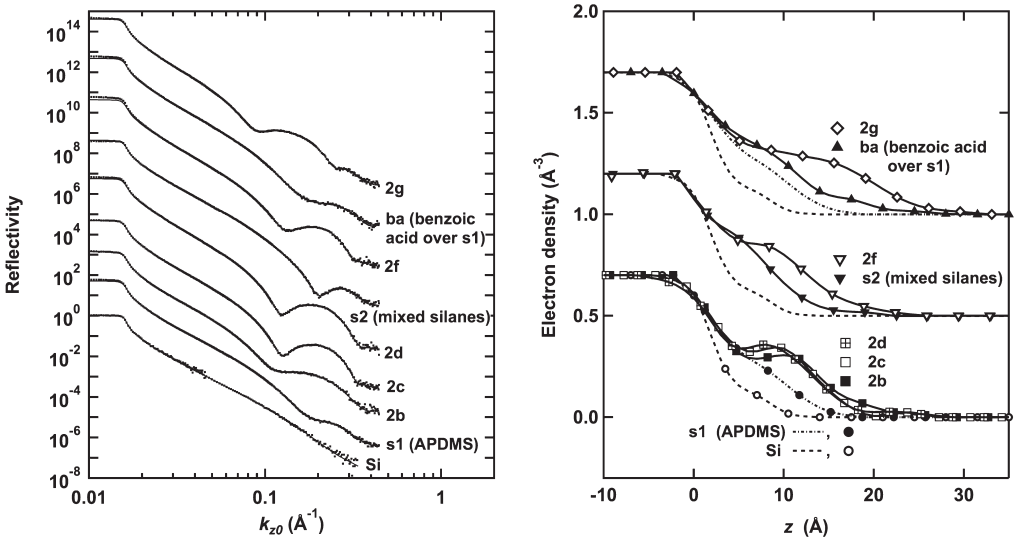

Figure 3. Analysis of the X-ray reflectivity of typical azobenzene monolayers. The sample codes are given in Table 1. (Left) Reflectivity (dots, data; lines, fits). The curves are displaced vertically for clarity. (Right) Electron density profiles from the fits of the XRR data. The Si/monolayer interface is located at 0 Å. The fitted values are given by the symbols; the continuous lines are drawn by cubic spline interpolation. The three sets of curves are displaced vertically by increments of 0.5 electron/Å^3.

the upper threshold above which grafted azobenzenes were shown not to isomerize anymore;[3] therefore, it is certainly large enough for our purposes.

Photoresponsive monolayer assemblies containing azobenzene derivative **2**, **3**, or **5** were fabricated by grafting the *N*-hydroxysuccinimide-activated ester derivatives onto the aminosilane monolayer (route 1) or by the direct reaction of the carboxylic acid group of **2** with the aminosilane monolayer in the presence of *N*-hydroxybenzotriazole (HOBt) (route 2). Figure 2 shows a typical XPS survey scan and high-resolution elemental C 1s scan that were recorded from a monolayer of **2** grafted by route 1. In addition to the peaks from the Si substrate, the survey scan exhibits N 1s (399.8 eV) and C 1s (284.8 eV) peaks with a relative intensity of 1:9, which is close to the 1:11.5 ratio of **2** and to the 1:8.6 ratio of **2** grafted to an aminopropyl moiety. The C 1s core-level spectrum of the monolayer of grafted **2** (inset of Figure 2) indicates the presence of three components having binding energies at about 284.8, 286, and 288.4 eV corresponding to C−(H,C), C−O/C−N, and (O═C)−N carbons, respectively. XPS thus fully confirms the grafting of the azobenzene molecules onto the silicon substrates.

Atomic force microscopy (AFM) images obtained on the monolayers were featureless, except for the presence of a few dust particles. Therefore, the structural quality of the monolayers was evaluated by X-ray reflectometry (XRR). The analysis involved finding the average thickness *d* of the monolayer from the final peak of the correlation function of the electron density gradient (i.e., the Patterson function), which was computed by Fourier transformation of the data scaled by the Fresnel reflectivity of the substrate.[38,39] This provided an accurate, parameter-free estimation of the thickness. In addition, the reflectivity was fit as described in the Experimental Section in order to obtain the vertical profiles of the electron density of the monolayers, $\rho(z)$. A series of such profiles are given in Figure 3, together with the reflectivity data. The successful grafting of the azobenzene molecules is readily confirmed by comparing the electron density profiles of the monolayers with that of a bare silicon wafer (Si in Figure 3) or the aminosilane monolayer (s1 in Figure 3).

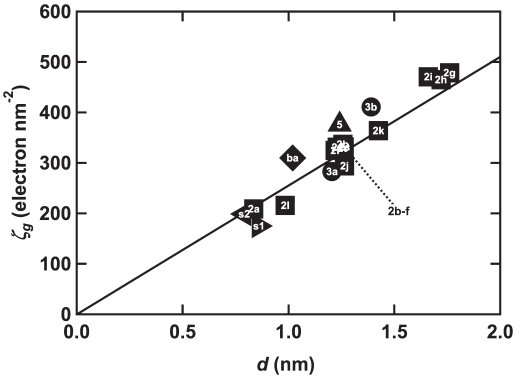

Figure 4. Correlation between the number of electrons per unit area of the monolayers (ζ_g, computed from the electron density profiles obtained by fitting the XRR data) and the average layer thickness of the monolayers (*d*, computed from a parameter-free analysis of the XRR data). All of the samples in this study are collected in the graph. The slope of the line provides the average electron density of the monolayers (255 ± 6 electrons/nm^3). Sample codes are given in Table 1.

From these profiles and a knowledge of the profile of a clean Si wafer, the number of electrons per unit surface in the monolayers (ζ_g) was computed by integration (details in Experimental Section). Figure 4 presents the variation of the integrated electron density ζ_g versus the average monolayer thickness *d* for all samples reported in this article, including simple silane monolayers and various azobenzene monolayers. Because thicker layers have a proportionally larger number of electrons per unit surface, ζ_g should vary linearly with *d*, as indeed observed. The good correlation between the thickness, which is extracted from a parameter-free analysis of the reflectivity curves, and the integrated intensity, which is obtained from the modeling of the data, provides a strong validation of the fitting procedure and of the extraction process of the number of electrons in the grafted layers. The line in Figure 4 has a slope of 255 ± 6 electrons/nm^3, which is slightly lower than the electron density of amorphous

dx.doi.org/10.1021/la201526u |*Langmuir* 2011, 27, 9403–9412

Table 1. Structural Parameters and Wetting Characteristics (Water) of Azobenzene-Based Monolayers

sample code	grafted molecule	comment	substrate	d(nm)[a]	ζ_g (electron /nm^2)[b]	σ_g (molecule/ nm^2)[c]	θ_{wat} (deg) (trans)[d]	$\Delta\theta_{wat}$ (deg) (cis−trans)[e]
s1	γ-aminopropyldimethyl-ethoxysilane (APDMS)		Si wafer	0.86	175	2.69	72	
s2	mixed monolayer: APDMS/ *tert*-butyldiphenylchlorosilane		Si wafer	0.79	199		70.5	
ba	NHS-activated benzoic acid		s1	1.02	310	2.45	69	
2a	NHS-activated **2**	incomplete reaction	s1	0.84	209	0.16	71	1
2b	NHS-activated **2**		s1	1.26	337	0.76	58	3
2c	NHS-activated **2**		s1	1.26	332	0.74	57	3.5
2d	NHS-activated **2**		s1	1.26	329	0.73	58.5	3.5
2e	NHS-activated **2**	grafted under UV irradiation	s1	1.23	331	0.74	57.5	4.5
2f	NHS-activated **2**	grafted over mixed monolayer	s2	1.22	325	0.59	58.5	6.5
2g	NHS-activated **2**	cografted with NHS-activated benzoic acid	s1	1.76	479	1.06	56.5	8
2h	NHS-activated **2**	previous, measured under visible irradiation	s1	1.72	465	0.97		
2i	NHS-activated **2**	previous, measured under UV irradiation	s1	1.66	471	1.01		
2j	**2** (HOBt activation)		s1	1.26	294	0.56	69.5	2.5
2k	**2** (HOBt activation)		s1	1.42	364	0.89	61	3.5
2l	**2** (HOBt activation)	lower concentration of **2**	s1	0.98	216	0.19	75	2
3a	NHS-activated **3**		s1	1.21	283	0.66	67	3
3b	NHS-activated **3**	cografted with NHS-activated benzoic acid	s1	1.39	411	0.91	65	5
5	NHS-activated **5**		s1	1.24	376	0.94	56.5	4.5

[a] Layer thickness from the analysis of the XRR Patterson function. [b] Number of electrons per unit area in the monolayer from the modeling of the XRR. [c] Number of molecules grafted per unit area. [d] Static water contact angle in the trans state. [e] Difference in water contact angles after 15 min of irradiation at 360 and 450 nm (cis and trans states).

polyethylene (294 electrons/nm^3). Therefore, the layers are amorphous and contain a substantial amount of free volume. The amorphous nature of the layers is also supported by the relatively small values of thickness, which are invariably lower than 2 nm, while the extended length of **2** coupled to aminopropylsilane is close to 3 nm.

The integrated electron densities ζ_g can be transformed as the number of molecules grafted per unit surface, σ_g, on the basis of the knowledge of the number Z of electrons in a molecule and of the ζ_g of the underlying silane monolayer. The values obtained for different grafting conditions are between ∼0.2 and ∼1.0 molecule/nm^3 (Table 1). This is significantly lower than the ∼2.7 amino groups/nm^2 of the silane monolayer. However, when NHS-activated benzoic acid was reacted on the aminopropylsilane monolayer, a much higher grafting density of 2.4 molecule/nm^2 was obtained, indicating quantitative reaction with the aminopropylsilane monolayer and showing that steric hindrance is the reason for the lower grafting of the bulky azobenzene molecules. Note that the reproducibility of the experiments was good, as confirmed by the close values obtained for three different monolayers of **2** (samples **2b**−**d**).

Photoresponsive Wetting Properties of Azobenzene Monolayers. The wettability of the different azobenzene-functionalized monolayers was studied by means of static water contact angle (WCA) measurements (Table 1). The WCA value of the aminosilane monolayer is 72° and decreases when the hydrophilic para-substituted azobenzenes are grafted. In general, monolayers of higher grafting density tend to display lower contact angles with water (Figure 5), which indicates that the hydrophilic extremities of the *trans*-azobenzenes tend to accumulate at the outer interface. However, the contact angles remain larger than expected if only hydrophilic groups are accumulating at the outer interface. For instance, the WCA of oligo(ethylene oxide) silane monolayers was reported to be ∼40°,[43] whereas it remains larger than 55° for monolayers of di(ethylene glycol)-substituted azobenzene **2**. This is in agreement with the XRR

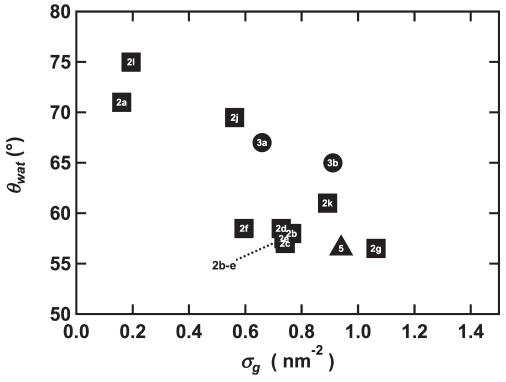

Figure 5. Correlation between the grafting density of hydrophilic para-substituted azobenzenes **2**, **3**, and **5** and the static water contact angle of the corresponding monolayers. Sample codes are given in Table 1.

dx.doi.org/10.1021/la201526u |*Langmuir* 2011, 27, 9403–9412

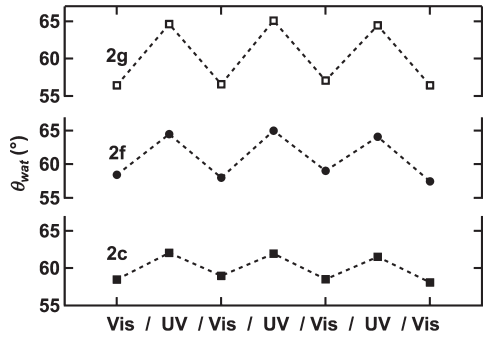

Figure 6. Contact angle of water on three different monolayers of azobenzene **2** after 15 min of irradiation with light of 450 and 360 nm wavelengths. The samples are described in Table 1; 2f and 2g are samples for which the azobenzene molecules are standing in a more upright orientation (Scheme 3).

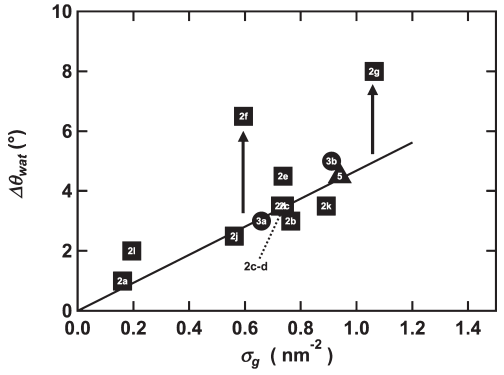

Figure 7. Difference in water contact angles of the azobenzene monolayers when the samples are irradiated with light of 360 and 450 nm wavelengths (cis vs trans configurations) vs the number of grafted azobenzene molecules per unit surface. The two arrows denote samples for which the azobenzene molecules are standing in a more upright orientation (Scheme 3). Sample codes are given in Table 1.

results that showed that the monolayers are amorphous and not densely packed. Therefore, the outer surface of the monolayers is amphiphilic.

The samples were successively irradiated at 450 and 360 nm for 15 min, and the average WCA was measured for each photoinduced state of the azobenzene monolayers (Figure 6). For all samples in this study, UV irradiation invariably resulted in an increase in the water contact angle, which could be reversibly switched back by irradiation with visible light. Hence, the layers are behaving as intended because they become less hydrophilic upon trans to cis isomerization, in contrast with most previous studies.

Figure 7 plots the difference in the contact angle between the cis and trans forms, $\Delta\theta_{wat}$, versus the number of azobenzene molecules grafted per nm^2, σ_g. Larger grafting densities correspond to larger $\Delta\theta_{wat}$, with a close-to-linear dependence between both parameters (except for samples 2f and 2g for which special grafting methodologies were used, see below). However, the variation in the water contact angle remains small, below ~4°.

The restricted change in wettability is not the result of steric hindrances that would prevent complete switching of the azobenzene molecules upon irradiation. Indeed, when azobenzene **2** was grafted in its cis form (under irradiation at 360 nm, sample 2e), no significant difference in the grafting density or wettability was observed compared with the same compound grafted in its trans configuration (samples 2b−d). Thus, we hypothesized that the low variation of WCA is more likely due to the amorphous nature of the monolayers and the tilted orientation of the azobenzene molecules; the change in the azobenzene configuration would then result only in a limited change in the composition of the outmost surface of the monolayers.

Engineering the Azobenzene Monolayers for an Improved Wettability Contrast. Therefore, two methodologies were used in order to force the azobenzene molecules to stand in a more upright orientation (Scheme 3). First, the aminosilane monolayer was straigthened by adding bulky molecules to the silane monolayer (sample s2). This involved coreacting γ-aminopropyldimethylethoxysilane and *tert*-butyldiphenylchlorosilane in order to decrease the degrees of freedom of the aminopropyl chains in the monolayer. Because the exact composition of the monolayer is not known, it is not possible to compute a grafting density anymore. However, the grafting density of azobenzene **2** over this mixed layer can still be computed by measuring the electron densities of the mixed silane layer before and after the grafting of the azobenzene. Interestingly, despite a slight decrease in the grafting density compared to that of standard monolayers, $\Delta\theta_{wat}$ increased to 6.5° (sample 2f in Table 1 and the first vertical arrow in Figure 7), confirming that a rigidification of the bottom silane layer is favorable to the wettability contrast.

Therefore, a second strategy was followed whereby NHS-activated azobenzene **2** was coreacted with NHS-activated benzoic acid over the aminosilane monolayer (sample 2g in Table 1 and the second vertical arrow in Figure 7). In this case, the inclusion of benzoic acid (which was shown above to react quantitatively with the aminosilane layer) densifies the bottom part of the monolayer of grafted azobenzene molecules (Scheme 3). Here again, it is possible to estimate the grafting density of azobenzene-modified monolayers by a comparison of the integrated electron density of this monolayer with that of a monolayer obtained by grafting NHS-benzoic acid only over the aminosilane monolayer. Compared to standard monolayers of **2**, a significant increase in the grafting density is observed with 2g (about 40%), together with an even larger increase in $\Delta\theta_{wat}$ from 3.5 to 8°; the monolayer thickness also increases by 0.5 nm (from ~1.2 to ~1.7 nm). These observations are in agreement with the improved vertical orientation of the azobenzene groups.

When the same strategy was applied to azobenzene **3**, the grafting density of the azobenzene moiety was again increased by about 40%, the contact angle was increased from 3.0 to 5.0°, and the thickness was increased from 1.2 to 1.4 nm (sample 3b vs sample 3a). Again, the structural results indicate that the molecules stand in a more upright orientation; the lower increase in the wettability contrast is obviously due to the difference of hydrophilicity between azobenzenes **2** and **3**. These observations fully confirm that the densification of the bottom part of the monolayer improves the wettability contrast between the trans and cis configurations and provides support for the notion that forcing azobenzenes into a more upright position is needed for an optimal photoresponse.

Finally, the effect of the trans−cis photoisomerization on the structure of sample 2g was measured by XRR under continuous visible or UV irradiation (Figure 8, samples 2h and 2i in Table 1). The X-ray reflectograms were very similar, indicating that both the thickness and the roughness of the monolayers are essentially not affected by the change in configuration of the

Scheme 3. Idealized Structures of Three Different Types of Monolayers Based on Azobenzene 2[a]

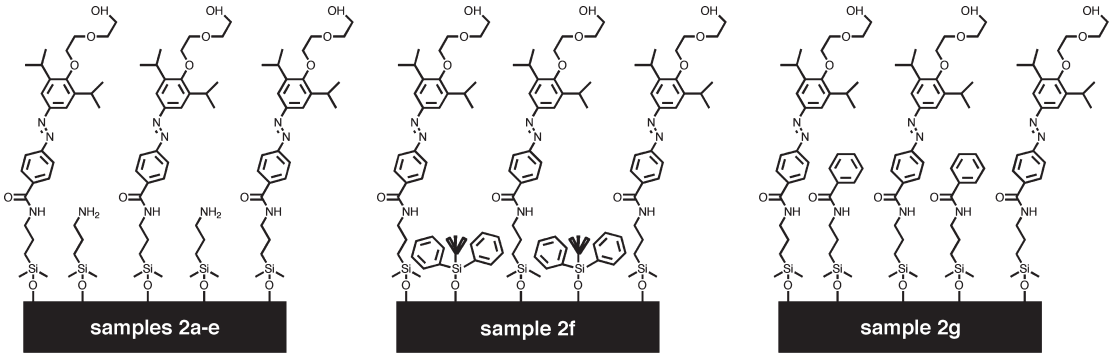

[a] Samples 2f and 2g are designed to favor the improved vertical orientation of the azobenzene groups.

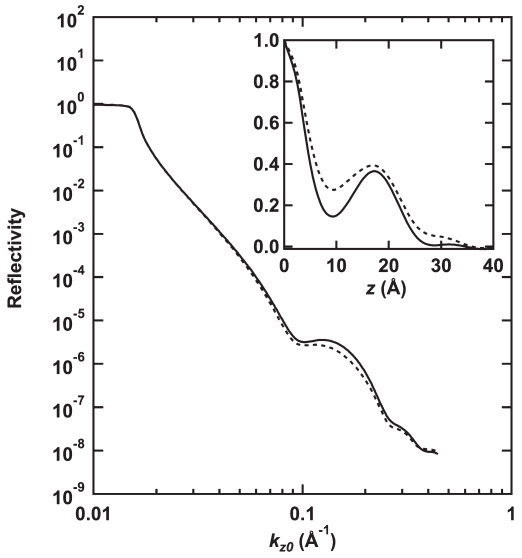

Figure 8. X-ray reflectivity of sample 2g measured under continuous UV irradiation (cis state, dashed line, sample 2i in Table 1) and then under continuous visible irradiation (trans state, continuous line, sample 2h in Table 1). The inset shows the corresponding Patterson functions (i.e., the autocorrelation functions of the electron density gradient profiles).

azobenzene molecules. Actually, a thickness decrease of only ~0.05 nm was observed in the XRR Patterson functions when switching from the trans to the cis configuration, which is hardly significant. Siewierski et al. reported an unexpected increase of 0.1 nm thickness between *cis*- and *trans*-azobenzene-silane monolayers.[14] Xing and Mattice[44] have simulated azobenzene monolayers and have predicted modest decreases in layer thickness upon isomerization, from 0 to 0.3 nm depending on the packing density of the layers. Our results are compatible with these previous studies and confirm that only very small variations in layer thickness and roughness can be obtained upon azobenzene photoisomerization.

CONCLUSIONS

We have assembled several photoresponsive monolayers on silicon oxide surfaces by grafting finely engineered azobenzenes onto preformed aminosilane monolayers. Monolayers with grafting densities in the 0.2−1.0 molecule/nm^2 range were readily obtained. These monolayers exhibited reversible photoisomerization, switching from a more to a less hydrophilic state upon UV irradiation. Our work shows that the wettability is not necessarily dominated by the change in the dipole moment of azobenzene but may originate from variations in the orientation of functional groups and the composition of the outmost surface. The possibility to reorient functional groups with light is of wide interest: the fine tuning of ortho, meta, or para substitutions of azobenzene, combined with proper monolayer engineering, can indeed offer new possibilities for building sophisticated light-triggered devices for applications in biology[5] and catalysis.[7]

Concerning wettability, the light-driven changes in the water contact angle correlate linearly with the grafting density but remain small (below ~4°). It is possible to increase the wettability contrast by forcing the molecules to stand in a more upright position, either by densifying the underlying aminosilane monolayer by cosilanation with a bulky silane or by filling the voids left at the bottom of the layer of grafted azobenzenes with a shorter aromatic molecule. In the latter case, the cis−trans difference in the contact angle can reach 8° and is in the upper range of values usually reported in the literature for azobenzene monolayers (although of opposite sign because most systems reported to date switch from a less hydrophilic trans state to a more hydrophilic cis state). The limited change in wettability might be due to a combination of factors. First, the lower hydrophobicity resulting from the composition change upon trans to cis isomerization is partially counterbalanced by the larger dipole moment of the cis form. Second, the rate of cis to trans thermal isomerization might be higher in the monolayers because of crowding, which would shift the equilibrium to lower cis contents.

In light of these results, it becomes obvious that very large light-driven changes in wettability are not to be expected for smooth azobenzene monolayers. The correlation plots obtained in this work suggest that reaching more than an ~10° difference in the contact angle is unlikely for these systems because it is known that the higher bound for easy switching of grafted azobenzene molecules is ~2.5 azobenzene molecules/nm^2. These moderate variations may nevertheless be sufficient for applications in microfluidics; in this specific context, our work provides handles to design efficient photoresponsive surfaces.

AUTHOR INFORMATION

Corresponding Author

*E-mail: alain.jonas@uclouvain.be.

Present Addresses
[†]State Key Laboratory of Solid Lubrication, Lanzhou Institute of Chemical Physics, Chinese Academy of Sciences, Lanzhou 730000, China.

■ ACKNOWLEDGMENT

We gratefully acknowledge access to the SUCH and ASM platforms of IMCN. B.N. is a senior research associate of the FRS-FNRS. Financial support was provided by the Communauté Française de Belgique (ARC 06-11/339), the Belgian Federal Science Policy (IAP-PAI P6/27), the F.R.S.-FNRS, and the Wallonia Region (Nanotic-Feeling).

■ REFERENCES

(1) Wang, S.; Song, Y.; Jiang, L. *J. Photochem. Photobiol., C* **2007**, *8*, 18–29.
(2) Browne, W. R.; Feringa, B. L. *Annu. Rev. Phys. Chem.* **2009**, *60*, 407–428.
(3) Klajn, R. *Pure Appl. Chem.* **2010**, *82*, 2247–2279.
(4) Ichimura, K.; Oh, S.-K.; Nakagawa, M. *Science* **2000**, *288*, 1624–1626.
(5) Auernheimer, J.; Dahmen, C.; Hersel, U.; Bausch, A.; Kessler, H. *J. Am. Chem. Soc.* **2005**, *127*, 16107–16110.
(6) Liu, D. B.; Xie, Y. Y.; Shao, H. W.; Jiang, X. Y. *Angew. Chem., Int. Ed.* **2009**, *48*, 4406–4408.
(7) Stoll, R. S.; Hecht, S. *Org. Lett.* **2009**, *11*, 4790–4793.
(8) Smaali, K.; Lenfant, S.; Karpe, S.; Ocafrain, M.; Blanchard, P.; Deresmes, D.; Godey, S.; Rochefort, A.; Roncali, J.; Vuillaume, D. *ACS Nano* **2010**, *4*, 2411–2421.
(9) Tamai, N.; Miyasaka, H. *Chem. Rev.* **2000**, *100*, 1875–1890.
(10) Irie, M. *Chem. Rev.* **2000**, *100*, 1683–1684.
(11) Ichimura, K.; Suzuki, Y.; Seki, T.; Hosoki, A.; Aoki, K. *Langmuir* **1988**, *4*, 1214–1216.
(12) Aoki, K.; Seki, T.; Suzuki, Y.; Tamaki, T.; Hosoki, A.; Ichimura, K. *Langmuir* **1992**, *8*, 1007–1013.
(13) Sekkat, Z.; Wood, J.; Geerts, Y.; Knoll, W. *Langmuir* **1995**, *11*, 2856–2859.
(14) Siewierski, L. M.; Brittain, W. J.; Petrash, S.; Foster, M. D. *Langmuir* **1996**, *12*, 5838–5844.
(15) Liu, N.; Dunphy, D. R.; Rodriguez, M. A.; Singer, S.; Brinker, J. *Chem. Commun.* **2003**, 1144–1145.
(16) Akiyama, H.; Tamada, K.; Nagasawa, J.; Abe, K.; Tamaki, T. *J. Phys. Chem. B* **2003**, *107*, 130–135.
(17) Hamelmann, F.; Heinzmann, U.; Siemeling, U.; Bretthauer, F.; Vor der Brüggen, J. *Appl. Surf. Sci.* **2004**, *222*, 1–5.
(18) Sortino, S.; Petralia, S.; Conoci, S.; Di Bella, S. *J. Mater. Chem.* **2004**, *14*, 811–813.
(19) Yang, D.; Piech, M.; Bell, N. S.; Gust, D.; Vail, S.; Garcia, A. A.; Schneider, J.; Park, C.-D.; Hayes, M. A.; Picraux, S. T. *Langmuir* **2007**, *23*, 10864–10872.
(20) Kawanishi, Y.; Tamaki, T.; Sakuragi, M.; Seki, T.; Suzuki, Y.; Ichimura, K. *Langmuir* **1992**, *8*, 2601–2604.
(21) Aoki, K.; Ichimura, K.; Tamaki, T.; Seki, T.; Kawanishi, Y. *Makromol. Chem.* **1992**, *193*, 2163–2174.
(22) Delorme, N.; Bardeau, J. F.; Bulou, A.; Poncin-Epaillard, F. *Langmuir* **2005**, *21*, 12278–12282.
(23) Zhang, X.; Wen, Y.; Li, Y.; Li, G.; Du, S.; Guo, H.; Yang, L.; Jiang, L.; Gao, H.; Song, Y. *J. Phys. Chem. C* **2008**, *112*, 8288–8293.
(24) Peor, N.; Sfez, R.; Yitzchaik, S. *J. Am. Chem. Soc.* **2008**, *130*, 4158–4165.
(25) Dietrich, P.; Michalik, F.; Schmidt, R.; Gahl, C.; Mao, G.; Breusing, M.; Raschke, M. B.; Priewisch, B.; Elsässer, T.; Mendelsohn, R.; Weinelt, M.; Rück-Braun, K. *Appl. Phys. A: Mater. Sci. Process.* **2008**, *93*, 285–292.
(26) Yasuda, S.; Nakamura, T.; Matsumoto, M.; Shigekawa, H. *J. Am. Chem. Soc.* **2003**, *125*, 16430–16433.
(27) Kumar, A. S.; Ye, T.; Takami, T.; Yu, B. C.; Flatt, A. K.; Tour, J. M.; Weiss, P. S. *Nano Lett.* **2008**, *8*, 1644–1648.
(28) Tamada, K.; Akiyama, H.; Wei, T. X. *Langmuir* **2002**, *18*, 5239–5246.
(29) Tamada, K.; Akiyama, H.; Wei, T. X.; Kim, S. A. *Langmuir* **2003**, *19*, 2306–2312.
(30) Ah Qune, L. F. N.; Akiyama, H.; Nagahiro, T.; Tamada, K.; Wee, A. T. S. *Appl. Phys. Lett.* **2008**, *93*, 083109.
(31) Kondo, T.; Kanai, T.; Uosaki, K. *Langmuir* **2001**, *17*, 6317–6324.
(32) Schlenoff, J. B.; Li, M.; Ly, H. *J. Am. Chem. Soc.* **1995**, *117*, 12528–12536.
(33) Baralia, G. G; Duwez, A.-S.; Nysten, B.; Jonas, A. M. *Langmuir* **2005**, *21*, 6825–6829.
(34) Radüge, C.; Papastavrou, G.; Kurth, D. G.; Motschmann, H. *Eur. Phys. J. E* **2003**, *10*, 103–114.
(35) *p*-Cyanoazobenzene monolayers have been suggested to be an exception because of the unusual fact that the dipole moment in the trans configuration is larger than in the cis configuration.[16] However, although a very slight increase in the water contact angle was reported upon the trans to cis isomerization of *p*-cyanoazobenzene,[16] a more recent report found the usual decrease in the water contact angle upon UV irradiation.[25]
(36) Lim, H. S.; Han, J. T.; Kwak, D.; Jin, M. H.; Cho, K. *J. Am. Chem. Soc.* **2006**, *128*, 14458–14459.
(37) Jonas, A. M.; Hu, Z.; Glinel, K.; Huck, W. T. S. *Nano Lett.* **2008**, *8*, 3819–3824.
(38) Bollinne, C.; Stone, V. W.; Carlier, V.; Jonas, A. M. *Macromolecules* **1999**, *32*, 4719–4724.
(39) Arys, X.; Laschewsky, A.; Jonas, A. M. *Macromolecules* **2001**, *34*, 3318–3330.
(40) Parratt, L. G. *Phys. Rev.* **1954**, *95*, 359–369.
(41) Lekner, J. *Theory of Reflection of Electromagnetic and Particle Waves*; Martinus Nijhoff: Dordrecht, The Netherlands, 1987.
(42) Segerman, E. *Acta Crystallogr.* **1965**, *19*, 789–796.
(43) Dekeyser, C. M.; Buron, C. C.; Mc Evoy, K.; Dupont-Gillain, C. C.; Marchand-Brynaert, J.; Jonas, A. M.; Rouxhet, P. G. *J. Colloid Interface Sci.* **2008**, *324*, 118–126.
(44) Xing, L.; Mattice, W. L. *Langmuir* **1996**, *12*, 3024–3030.